RADAR MEASUREMENTS AND ANALYSES OF SPENT ARIANE ROCKET BODIES IN GEOSTATIONARY TRANSFER ORBITS

L. Leushacke

Research Institute for High Frequency Physics (FHP),
Research Establishment for Applied Science (FGAN), Wachtberg-Werthhoven, Germany

ABSTRACT

Spent upper rocket stages remaining in geostationary transfer orbits (GTO) pose a severe hazard to space activities in most operational altitudes. Assessment and monitoring of their actual state and prediction of its future development is complicated by the special features of GTOs, like fast orbit changes, strong atmospheric influence dependance near perigee and visibility and sensitivity constraints of ground-based sensors. The reliability of orbital lifetime predictions depends on the accuracy by which their physical characteristics like orbit, attitude, size, shape, mass and material properties can be determined.

From measurements on selected ARIANE upper stages and analyses of the collected data it will be shown, to which degree actual physical characteristics of upper stages in GTO may be assessed by ground-based radars like the FGAN High Power Radar System.

1. INTRODUCTION

Launch systems used for missions in higher Earth orbits and the geostationary ring contribute a large number of operational debris to the current debris environment. Especially upper rocket stages remaining in geostationary transfer orbits (GTO) like the ARIANE 3rd stages may increase the hazard to space activities due to several reasons: They are typically of large size and mass and their orbital lifetimes range from several years to more than 100 years. There is a high risk of secondary debris production by explosions due to residual fuel. As perigee height is low (about 200 km) and apogee nearly reaches the geostationary ring (36000 km), upper stages in GTO pass most operational altitudes. Furthermore, their monitoring by Earth based sensors is complicated by fast orbit changes, caused by strong atmospheric influences near perigee, and by limited sensivity and visibility constraints.

Since December 1979 there have been 50 successful launches with ESA's ARIANE 3-stage launch system (status of 1/93 (Ref. 1)). 9 upper stages have decayed and 1 is known to be exploded. This high intensity explosion of the AR1-11 in November 1986 produced about 500 debris objects, of which about 60 are still tracked in orbit. Currently 35 ARIANE upper stages (1 AR1, 4 AR2, 8 AR3 and 22 AR4) in GTO are regularly tracked by the USSPACECOM Space Surveillance Network (SSN) and their orbital parameters are distributed as two-line element sets (TLE).

Besides orbital parameters, more detailed information concerning the actual physical properties of the stages is needed for risk assessments and precise orbital lifetime predictions. It is important to know, whether they are still intact or have fragmented and if they are in a stable or rotational mode. No such information is reported up to now. The main objectives of the present work are: To which degree may physical characteristics of upper stages in GTO be assessed from measurements with radars like the FGAN High Power Radar System?

In section 2 some of the general and FGAN site and system specific restrictions for observing GTO objects by ground-based sensors are discussed. Some of the methods used for incoherent analysis of radar returns are outlined and demonstrated in section 3. Measurements performed with the FGAN radar on selected ARIANE upper stages as well as examplaric analyses results are summarized in section 4.

2. GTO OBSERVATION CONSTRAINTS

2 1 General considerations

The observability of objects in GTO by ground-based sensors is complicated by the special features of geostationary transfer orbits. Some of the relevant characteristics are listed in Table 1 for the standard GTO of ARIANE (Ref. 2).

ecentricity	e	=	0.73
perigee height	h_P	=	200 km
apogee height	h_A	=	35786 km
inclination	i	=	7^o
argument of perigee	ω	=	180^o
mean motion	n	=	2.275 1/day
secular pertubations due to earth oblateness			
argument of perigee	$\Delta\omega$	$\approx$	0.82^o/day
right asc. of node	$\Delta\Omega$	$\approx$	-0.42^o/day

Table 1. Initial orbital parameters of ARIANE GTO

Table 1 shows that observability of GTO objects strongly depends on sensor location (best near equator) and system sensivity (high slant ranges).

2.2 FGAN radar observation of GTO targets

Besides the general restrictions of GTO observation, additional limitations caused by sensor system location and characteristics must be regarded.

1. The FGAN High Power Radar System
The Research Establishment for Applied Science (FGAN) operates a High Power Radar System about 20 km south of Bonn, Germany. It consists of a L-band (1.333 GHz) monopulse tracking radar and a Ku-band (16.7 GHz) high-resolution imaging radar, both simultaneously operating on the same target.

2. Visibility and observation parameters
Due to the FGAN site location at more than 50^o northern lattitude, all radar measurements of GTO targets are characterized by high slant ranges (> 6000 km), so that they belong to the class of radar critical targets. Problems with refraction and transmission losses caused by the low radar elevation angles (< 15^o) have to be taken into account. Sensivity analysis and tests show, that in the current configuration only the L-band radar is capable of measuring ARIANE upper stages in GTO.

3. Target search limitations
Since the L-band tracking radar has only limited search capabilities, accurate actual TLE sets are needed for target acquisition. These are gained by the USSPACECOM SSN and retrieved via ESA/ESOC at regular time intervals (about 3 times per week). Since they may be outdated or erroneous in case of GTO objects due to fast orbit changes (atmospheric influences in perigee region), target detection and acquisition sometimes may fail. Detailed analyses, using orbit prediction theories of BROUWER and LYDDANE, show that TLE sets used for GTO target acquisition should on average not be older than about 5 - 6 days.

4. PRF considerations
The minimum radar pulse repetition frequency (PRF), which is necessary to avoid undersampling of the target is determined by the following formulas (Refs. 3, 4). For the case of a stabilized object at slant range R with orbital velocity v one finds

$$f_{pr} \geq \frac{2\, L_{max}\, v}{\lambda\, R} \qquad (1)$$

and for a target rotating with period T_{rot}

$$f_{pr} \geq \frac{4\,\pi\, L_{max}}{\lambda\, T_{rot}} \; . \qquad (2)$$

Herein L_{max} is the targets maximum dimension and λ the radar wavelength. The minimum necessary PRF is given by the greater one of the two values. On the other hand, the PRF is absolutely limited by transmitter tube duty cycle and receive/transmit pulse management constraints. Thus the radar signatures of some objects may be undersampled (especially big, fast rotating GTO stages) and special methods to deal with these cases have to be considered.

3. ANALYSIS OF RADAR RETURNS

Each received L-band radar echo contains measures of the target position (azimuth, elevation and slant range), its range rate as well as amplitude and phase of the scattered wavefield. In this section some of the methods used for incoherent analysis of the data collected by the L-band radar with PRF are outlined and demonstrated with examples (see also Refs. 6-11). Coherent methods are not considered here, since the coherence properties of the L-band system will have to be investigated first.

3.1 The intrinsic motion problem

The radar cross section (RCS) of the target, calculated from the measured scatter data, is in general a function of the observed target aspect, which continuously changes with time as a result of orbital and intrinsic motion of the object:

$$\sigma(t) = \sigma(\,\varphi(t), \psi(t)\,) \; , \qquad (3)$$

where φ and ψ are the observation direction angles in a satellite-fixed coordinate system. These aspect angles as a function of time have to be determined, before a detailed signature analysis can take place. The aspect angle variation due to orbital motion may be calculated from the tracking data (azimuth, elevation). Thus the essential task is the determination of the targets intrinsic motion properties. This is in general however, only possible for a certain class of tumbling and spin-stabilized objects. In the case of a monostatic radar and incoherent data analysis there are even more restrictions: The target has to be rotational symmetric, so that the aspect may be described by one angle θ (the angle between axis of symmetry and radar-line-of-sight). The signature must at least show 4 specular returns from simple body parts (e.g. from cylinder wall, θ=90°). The intrinsic motion parameters and the aspect angle function $\theta(t)$ is found by iterative solution of a system of nonlinear equations (Ref. 5). It can be shown, that for good convergence a high sample frequency is necessary, in some cases much higher than the minimum PRF as determined by Eqs. 1 or 2.

3.2 Signature analysis methods

1. Size determination from specular returns
If the signature shows specular returns from object parts of known or assumed shape, the size of these parts may be determined in a very simple way. For the case of a cylinder, its length l and radius a are calculated from the peak RCS σ_s and the 3 dB angular width $\Delta\theta$ of the specular beam:

$$\begin{aligned} \sigma_s &= 2\,\pi\,\frac{a\,l^2}{\lambda} \\ \Delta\theta &= 0.44\,\frac{\lambda}{l} \end{aligned} \qquad (4)$$

2. Fourier analysis

For the case of a rotating target, its rotation periods are determined from the autocorrelation function of the signature. Other parameters which are gained from RCS Fourier analysis are the aspect angle dependend cross-range dimensions of the object. This technique, which is based on a windowed Fourier transform of the signature, or equivalently the autocorrelation function of the scattering aperture (Ref. 5), is demonstrated in Fig. 1. Fig. 1(a) shows a measured signature of the radar calibration satellite RADCAT, which is basically a cylinder (l=2.44m, a=0.61m) with elliptical half-caps (h=0.305m) on both ends. The calculated aspect angle is shown in Fig. 1(b). The windowed Fourier transform (Hamming window of 15° width, window center at θ=90°) in Fig. 1(c) gives a cylinder length of l≈2.6m.

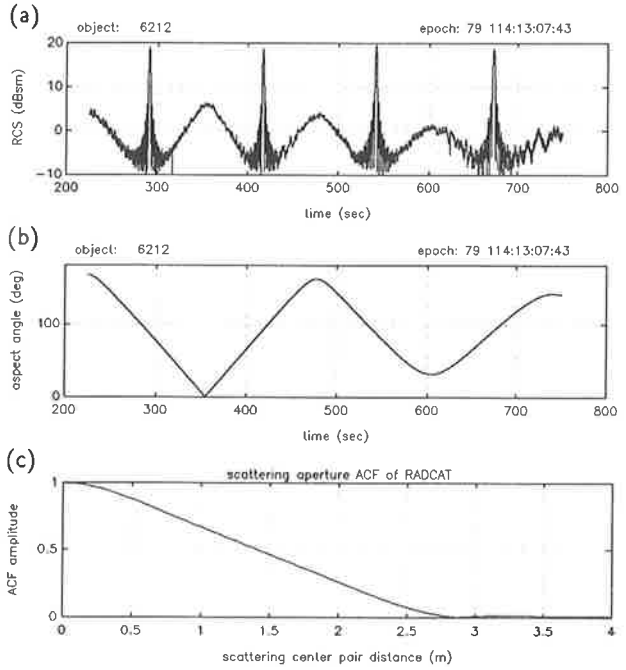

Figure 1. Signature Fourier analysis demonstration example. (a) L-band signature of RADCAT. (b) calculated aspect angle $\theta(t)$. (c) windowed signature Fourier transform (Hamming, θ=90°, $\Delta\theta$=15°).

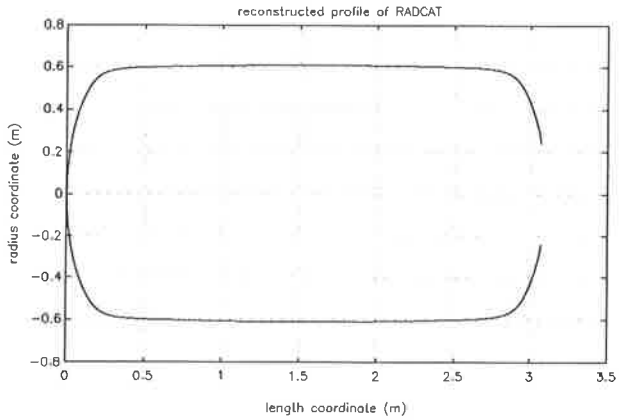

Figure 2. Profile reconstruction of RADCAT.

3. Profile reconstruction

If one finds signature parts, where the aspect angle linearly varies from 0 to 180° or vice versa, the objects profile function in its rotation plane may be calculated by inverse scattering techniques in geometrical optics (GO) approximation (Refs. 5,10,11). This method works well in case of purely convex objects as is demonstrated in Fig. 2, which shows the reconstructed profile of RADCAT calculated from the first linear aspect part (230 to 360 sec) of the signature of Fig. 1. The profile is not closed at the right end, since the aspect angle does not fully reach 180°. Shape and dimensions of RADCAT are reconstructed very well. It must be stated however, that in case of concave and focussing object parts or edges this method may lead to erroneous or even uninterpretable results.

4. Multi-period overlaying

It has been stated in section 2, that some signatures may be undersampled due to PRF limitations. In case of fast rotating objects, where the signature shows many rotation periods in a time interval in which aspect angle variation due to orbital motion may be neglected, a denser sampled signature may be achieved by projecting n successive periods onto the base interval. This method is demonstrated in Fig. 3. The upper diagram (a) shows a (simulated) undersampled signature of RADCAT. The sample frequency is 1 Hz, which in this case means 1 sample/7.2°. The effect of undersampling is easy to recognize from the periodically varying height of the 20 specular returns (which should all have a peak height of 20 dBsm). The result of overlaying of the 10 periods is shown in the lower diagram (b). The base period is resolved with 1 sample/0.36° and the analysis methods proposed above may now be applied.

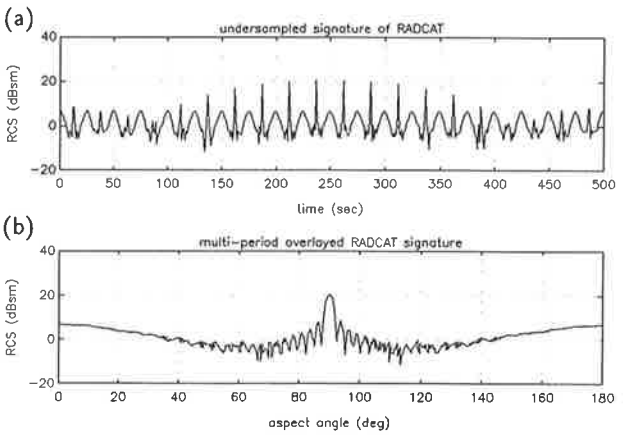

Figure 3. Multi-period overlaying simulation example. (a) Undersampled signature of RADCAT. (b) Overlay of all 10 periods.

5. RCS modelling

If the objects profile function is known in detail, theoretical signatures may be calculated for any assumed aspect angle variation by GO scattering techniques (Refs. 8,9). The input aspect angle function is then varied until the calculated signature fits best to the measured one. Again this method is limited to purely convex bodies and is seen to fail in the case of ARIANE rocket bodies.

6. RCS statistics
Assignment of aspect angles is limited to a very restricted class of objects as stated above. Global characterization and identification of scattering mechanisms may be achieved with statistical methods (Ref. 8). SWERLING and mixed distribution models are commonly used and lead to good results for the case of fluctuating and rotating targets. The critical initial assumption is however, that the aspect angle is equally distributed in $[0, 2\pi]$. It will be seen later, that this condition is not fullfilled for the measurements of ARIANE stages in GTO.

4. MEASUREMENTS AND ANALYSIS RESULTS

4.1 ARIANE upper stage geometry

The main part of the ARIANE third stage is the cylindrical rocket body, which contains the liquid oxygen and hydrogen fuel tanks. The lengths of the main cylinder (diameter 2.6 m), which differ between the measured stage types (AR1, AR3 and AR4), are listed in Table 2 (see also Ref. 12). In the last column of Table 2 the expected peak RCS of specular returns from the cylinder walls as calculated from Eq. 4 are tabulated.

Attached to the rear is the HM7 third stage engine. From a radar point of view, the most critical part of the third stage is the SPELDA, ARIANE's dual launch system, whose lower half remains on top of the main body after successful separation of the payload(s). This concave structure, together with the complex payload adaptor inside, may be responsible for focussing effects and multiple reflections, which cannot effectively be modelled with the techniques discussed in section 3.

type	L_c (m)	L_{tot} (m)	σ_s (dBsm) *
AR-1	8.6	10.8	34.3
AR-3	9.9	12.1	35.5
AR-4	9.9	12.1	35.5
AR-4 H10+	10.2	12.4	35.8

* expected peak height, see Eq. 4.

Table 2. Dimensions of ARIANE third stage types.

4.2 Stages analysed

The different ARIANE upper stages, which have been measured and analysed, are listed in Table 3. Expected orbital lifetimes and predicted decay dates in Table 3 are taken from the *ESA bulletin of space objects* of 1/93 (Ref. 1). Although object 16615 is not in a geostationary transfer orbit (800 km circular sun-synchronous), it has been included in the analyses, since observations are available before and after explosion of the AR1-11. Fig. 4 shows typical signatures of object 16615 one week prior to breakup (a) and about 3 years later (b) (see also Ref. 6). Comparison of these measurements with observations of the other stages may give some hints about intactness and intrinsic motion behaviour.

COSPAR design.	sat. num.	name	expected lifetime	no. of meas.
86 019 C	16615	AR1-11	E 11/86	2/16 *
86 026 C	16657	AR3-06	100 y	7
88 063 C	19332	AR3-09	> 2003	5
88 081 C	19485	AR3-10	50 y	7
89 020 C	19877	AR4-03	D 4/92	4
89 041 C	20042	AR4-05	7/96	2
89 053 B	20123	AR3-11	3/94	3
92 021 C	21941	AR4-22	100 y	2

* before/after explosion of AR1-11

Table 3. Measured ARIANE upper stages.

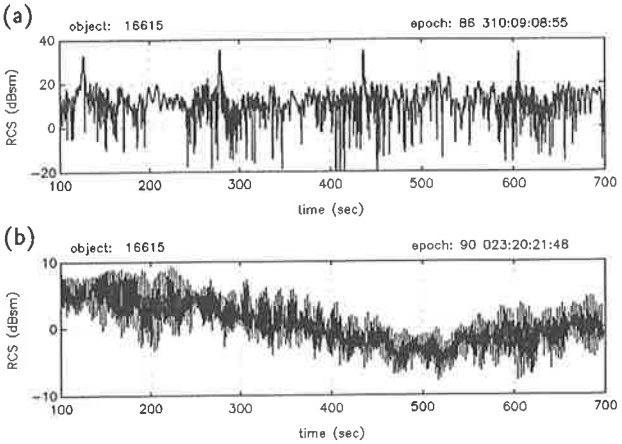

Figure 4. Typical L-band signatures of object 16615 before (a) and after (b) explosion. Time is given relative to epoch, RCS is scaled in decibel above one square meter (dBsm).

4.3 Analyses results

Detailed analyses of all measurements using the methods proposed in section 3 show, that the 8 upper stages may be roughly devided into two classes with respect to their signature characteristics and intrinsic motion behaviour.

Class I is constituted by objects 16615 (before explosion), 19877, 20042 and 21941. All measurements of these stages show characteristical specular returns of the main cylinder body (Fig. 5).

The cylinder dimensions, as calculated by various methods (section 3), coincide with the ones listed in Table 2. Thus at least the main cylinder bodies of these stages must be intact (must have been intact before explosion/decay in case of object 16615/19877 respectively). From the overshot in the specular return peak RCS in case of objects 19877, 20042 and 21941 (compare expected values in Table 2 with measured RCS in Table 4) it may be concluded, that their SPELDA hull is intact too.

Fig. 6 shows a result of the aspect angle determination algorithm, which is again typical for all four stages of this class. The relatively small variation of θ around the 90° aspect (sideview) indicates, that the intrinsic motion might be a tumbling in form of pre-

cession of the main body axis, possibly accompanied by spinning. Since the specular returns are slightly undersampled, the multi-period overlaying technique has been applied.

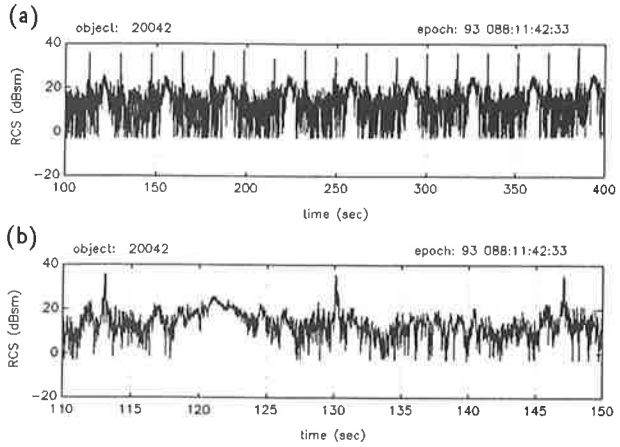

Figure 5. Typical L-band signature of class I objects. (a) RCS of complete observation interval. (b) Zoomed RCS plot showing one complete period.

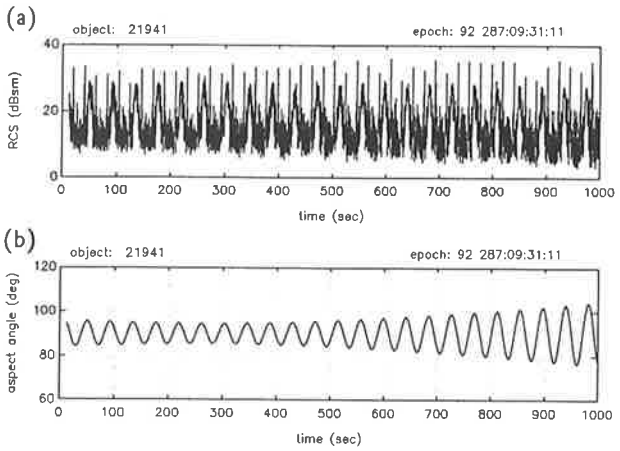

Figure 6. L-band signature of object 21941 (a) and calculated aspect angle variation (b).

Some of the results for class I stages are summarized in Table 4.

object number	max. RCS (dBsm) *	calc. dim. L, D (m)	rotation period (s) ⋆
16615	34.2	8.9, 2.7	350 ◇
19877	37.2	10.6, 2.8	26
20042	37.1	10.4, 2.7	34
21941	37.7	11.1, 2.7	42

* average of all observations
⋆ as of most recent observation
◇ before explosion

Table 4. Analysis results of class I stages.

Class II is constituted by objects 16657, 19332, 19485 and 20123, which are all still in GTO. The measured signatures of these stages show a more or less fluctuating RCS, but no specular returns (Fig. 7). Their intrinsic motion parameters can thus not be assessed with the methods presented in section 3 and a decision whether these stages are intact or fragmented cannot be made from signature analysis. If we assume however, that they are still intact, their most probable attitude might be a gravity gradient stabilized mode in combination with a precession or spinning. This may be supported by the fact, that these stages are in GTO since more than four years, so that they might have lost their initial rotational energy due to dissipation effects (Refs. 5,6). A gravity stabilized attitude may then be reached, if the mass distribution differs to a large amount between front and rear ends of the stage. Analyses results for the four class II stages are summarized in Table 5.

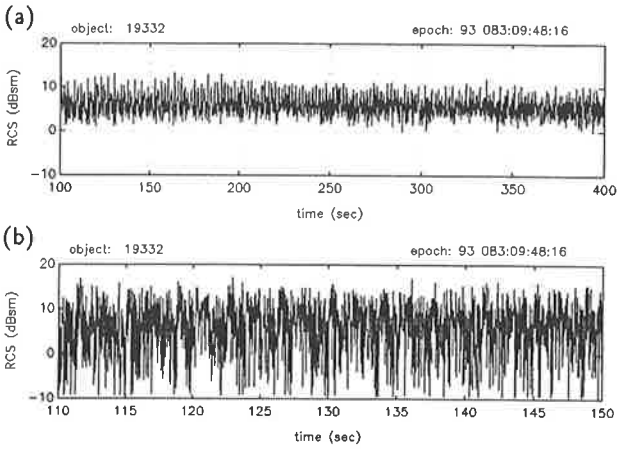

Figure 7. Typical L-band signature of class II objects (here obj. 19332). (a) RCS of complete observation interval (low pass filtered). (b) Zoomed signature section (unfiltered).

object number	mean RCS (dBsm) *	rotation period (s) ⋆
16657	17.2	10
19332	14.9	4
19485	15.6	-
20123	13.0	-

* average of all observations
⋆ as of most recent observation

Table 5. Analysis results of class II stages.

5. SUMMARY AND OUTLOOK

The special features of geostationary transfer orbits impose severe limitations to the observation of upper stages in GTO by ground-based radars like the FGAN radars. Measurements, which have been performed on selected ARIANE third stages, are currently restricted to the more sensitive L-band radar of FGAN. A variety of methods for incoherent analyses of the received echoes has been presented, by which at least some hints about the actual state of

the targets and their intrinsic motion behaviour may be gained. For more detailed information on their actual physical characteristics and precise mass estimation and lifetime prediction, a greater number of measurements over longer time periods would be necessary.

Some possibilities for improved measurement and analyses of GTO objects may be considered. Coherent signature analysis methods will be applicable, when detailed analyses and tests will have clarified the coherence properties of the L-band system. The development and implementation of incoherent and coherent pulse integration techniques and the refinement of detection strategies are currently under investigation at FGAN-FHP. The most important step however would be a sensivity enhancement of the Ku-band imaging radar, which provides high range resolution.

6. ACKNOWLEDGEMENTS

The author is indebted to the radar team at the FGAN-FHP High Power Radar System Division for having performed the large number of ARIANE upper stage measurements and to Dr. D. Mehrholz for many fruitful discussions.

7. REFERENCES

1. *ESA bulletin of space objects*, issue 13, 1/93, ESA/ESOC/MOD/MAS 1993.

2. Flury, W., *Vorlesung Raumfahrtmechanik*, ESA/ESOC, Darmstadt 1992.

3. Berkowitz, R. S., *Modern Radar*, J. Wiley & Sons, New York 1965.

4. Currie, N. C. (ed.), *Radar Reflectivity Measurement: Techniques & Applications*, Artech House Inc., Norwood 1989.

5. Gniss, H. and Magura, K., Analyse von inkohärenten Radarsignaturen eines taumelnden, rotationssymmetrischen Satelliten, *FGAN-FHP Forschungsbericht 7/82*, Wachtberg 1982.

6. Leushacke, L. and Mehrholz, D., Determination of physical characteristics of space debris, *Intermediate Reports No. 1-3, DARA Contract 50 ST 9003*, FGAN-FHP, Wachtberg 1991/92.

7. Bhattacharyya, A. K. and Sengupta, D. L., *Radar Cross Section Analysis & Control*, Artech House Inc., Norwood 1991.

8. Crispin, Jr., Siegel, K. M., *Methods of Radar-Cross-Section Analysis*, Academic Press, New York 1968.

9. Knott, E. F., Schaeffer, J. F. and Tuley, M. T., *Radar Cross Section*, Artech House Inc., Norwood 1985.

10. Weiss, M. R., Inverse scattering in the geometric-optics limit, *J. Opt. Soc. Am*, Vol. 58, p. 1524-1528, 1968.

11. Lewis, R. L., Physical optics inverse diffraction, *IEEE Trans. Anten. Propag.*, Vol AP-7, p. 308-314, 1969.

12. Hallmann, W. and Ley, W., *Handbuch der Raumfahrttechnik*, Hanser Verlag, München 1988.